PCCP

Ion Molecule Reactions in the HBr+ + HCl (DCl) System: A combined experimental and theoretical study

Journal:	*Physical Chemistry Chemical Physics*
Manuscript ID	CP-ART-08-2022-003654.R1
Article Type:	Paper
Date Submitted by the Author:	28-Nov-2022
Complete List of Authors:	Plamper, Dominik; Philipps Universität Marburg, Fachbereich Chemie Fujioka, Kazuumi; University of Hawai'i at Manoa, Chemistry Schmidt, Sebastian; Philipps Universität Marburg, Fachbereich Chemie Sun, Rui; University of Hawai'i at Manoa, Chemisty Weitzel, Karl-Michael; Philipps Universität Marburg, Fachbereich Chemie

ARTICLE

Ion Molecule Reactions in the HBr^+ + HCl (DCl) System:

A combined experimental and theoretical study

Received 00th January 20xx,
Accepted 00th January 20xx

DOI: 10.1039/x0xx00000x

Dominik Plamper,[a ‡] Kazuumi Fujioka,[b ‡] Sebastian Schmidt,[a ‡] Rui Sun, *[b] and Karl-Michael Weitzel,*[a]

Reactions in the system HBr^+ + HCl (DCl) were investigated inside a guided ion-beam apparatus under single-collision conditions. In the HBr^+ + HCl system are the proton transfer (PT_{HCl}) and charge transfer (CT) are observable. In the HBr^+ + DCl system proton transfer (PT_{DCl}) and deuterium abstraction (DA) are accessible. Cross sections for all reaction channels were measured as a function of the collision energy E_{cm} and of the rotational energy E_{rot} of the ion. The rotationally state-selective formation of the ionic species was realized by resonance-enhanced multiphoton ionization (REMPI). As expected, the PT-channels are exothermic, the cross section decreases with increasing collision energy for both PT_{HCl} and PT_{DCl}. The cross section for DA also decreases with increasing $E_{c.m.}$. In case of the considerably endothermic CT-channel, the reaction efficiency increases with increasing collision energy but has an overall much smaller cross sections compared to PT and DA reactions. Both PT-reactions are hindered by ion rotation, whereas DA is independent of E_{rot}. The CT-channel shows a rotational enhancement near the thermochemical threshold. The experiment is complemented by theory, using *ab initio* molecular dynamics (AIMD, also known as direct dynamics) simulations and taking the rotational enhancement of the HBr^+ into account. The simulations show good agreement to the experimental results. The cross section of PT_{HCl} decreases by an increase of the rotational energy. Furthermore the absolute cross sections are in the same order of magnitude. The CT reaction shows no reactions in the simulation.

Introduction

The investigation of ion-molecule reactions (IMRs) is important for understanding chemical processes in a variety of areas. For example, IMRs occur in the interstellar medium and in planetary ionospheres.[1] In this context, ion-molecule reactions between N^+, N_2^+ and CH_4, C_2H_2, C_2H_4 have been studied intensively in recent decades.[2–5] These are key reactions in the formation and chemical evolution of the atmosphere of Titan, which is the largest moon of Saturn. Due to remarkable parallels between the atmospheres of earth and Titan, the chemical processes in Titan's atmosphere are of great interest.[6] Besides IMRs based on cations, reactions with anions are of importance in interstellar space as well.[1]

A prominent example of IMRs in the interstellar medium is the reaction $H_2^+ + H_2 \rightarrow H_3^+ + H$. It is the precursor for a large part of the chemistry that occurs in dense interstellar clouds.[7] Since the temperature in these clouds is very low (≈ 10 K),[8] cold ion-molecule chemistry is an important research area. In this context, Merkt and co-workers studied the above mentioned reaction between H_2^+ and H_2 using a merged-beam approach.[9] Further approaches concerning cold ion-molecule chemistry are based on coulomb crystallization of ions in a trap[10] as well as on laser-induced reactions in a cold trap.[11] Because of the low temperatures in the interstellar medium, small changes of energy concerning the electronic, vibrational or rotational quantum states of reactants can change the outcome of reactions significantly.[8] IMRs also play an important role in plasma chemistry.[12–14] Furthermore, they find application in chemical ionization mass spectrometry (CI-MS)[15] and proton transfer reaction mass spectrometry (PTR-MS).[16]

While the influence of the collision energy on the cross section is in general well understood,[17] the current work focuses on the influence of external ion rotation on reactive cross sections (σ). In this context, resonance-enhanced multiphoton ionization (REMPI) offers the possibility to prepare rotationally state-selected ions. Based on this approach, several IMRs have been studied so far. Some reactions are hindered by increasing rotational energy, as for example the prominent reaction $H_2^+ + H_2 \rightarrow H_3^+ + H$.[18] Other reactions are independent of ion rotation. This applies to the charge transfer (CT) between H_2O^+ and CO[19] as well as the charge transfer between N_2^+ ($v^+ = 1, 2$) and Ar,[20] where v^+ represents the vibrational quantum state of N_2^+.

There are also reactions which show a rotational enhancement, such as the hydrogen/deuterium abstraction (HA/DA) between

[a] Philipps-Universität Marburg, Fachbereich Chemie, 35032 Marburg, Germany.
[b] Department of Chemistry, University of Hawai'i at Manoa, Honolulu, Hawaii 96822, United States
[c] * Karl-Michael Weitzel, weitzel@chemie.uni-marburg.de
[d] * Rui Sun, ruisun@hawaii.edu
Electronic Supplementary Information (ESI) available: [details of any supplementary information available should be included here]. See DOI: 10.1039/x0xx00000x
‡ Contributed equally to this work.

H_2O^+ and H_2/D_2/HD, investigated by Ng and co-workers.[21–23] Another example is the slightly endothermic reaction $H_2^+ + Ne \rightarrow NeH^+ + H$, which shows a rotational enhancement near the thermochemical threshold.[24] We will come back to this specific reaction later.

Rotational effects are expected to be large in systems where the ionic species has a large rotational constant. This is e.g. the case for hydrogen halide ions. In a previous study of Paetow et al., the considerable spin-orbit splitting of the ionic ground state of HBr^+ was utilized to investigate the exothermic proton transfer (PT) between HBr^+ ($^2\Pi_{1/2}$) and CO_2 as well as the endothermic proton transfer between HBr^+ ($^2\Pi_{3/2}$) and CO_2. Both reactions are hindered by ion rotation.[25,26]

In another study of Uhlemann et al., self-reactions in the HCl^+ (DCl^+) + HCl system were investigated as a function of the rotational energy in the HCl^+ ion. For the PT/HA and DT/HA channel the results suggested a minimum of the cross section σ in the rotational energy region where the rotational velocities of the ion and the neutral molecule (ω_{ion} and $\omega_{neutral}$) are approximately equal. The cross section of the CT-channel increases modestly with increasing rotational energy.[27,28]

Furthermore, for the HCl^+ + HCl system *ab initio* molecular dynamics (AIMD, also known as direct dynamics) simulations have been performed by Luo et al..[29] For the proton transfer reaction the normalized cross sections of the theoretical and experimental results showed nearly the same collision energy dependence. In addition, for the charge transfer reaction both theoretical and experimental normalized cross sections displayed a maximum at the same collision energy of 0.5 eV.[29]

In a recent work, Schmidt et al. reported on self-reactions in the HBr^+ (DBr^+) + HBr system. In case of PT/HA and DT/HA, σ runs through a minimum as function of the rotational energy of the ion as well, but in contrast to the HCl^+ (DCl^+) + HCl system, the positions of the minima do not correlate with the ratio $\omega_{ion}/\omega_{neutral}$. The cross section of the CT-channel increases considerably with increasing rotational energy.[30]

Stimulated by these versatile results, this work extends the research on hydrogen halides by reporting the rotational and translational dependence of HBr^+ ($^2\Pi_{1/2}$) + HCl (DCl) reactions. The following reaction channels were investigated:

$HBr^+ + HCl \rightarrow Br + H_2Cl^+$ (PT_{HCl}) ($\Delta H = -0.51$ eV)[31]
$HBr^+ + HCl \rightarrow HBr + HCl^+$ (CT) ($\Delta H = +0.76$ eV)[31]
$HBr^+ + DCl \rightarrow Br + HDCl^+$ (PT_{DCl}) ($\Delta H = -0.56$ eV)[31–33]
$HBr^+ + DCl \rightarrow HDBr^+ + Cl$ (DA) ($\Delta H = -0.002$ eV)[31,33,34]

Here, the thermochemistry given refers to the respective spin orbit ground state of the open shell product species. In case of HBr^+ + HCl, the HA-reaction cannot be investigated as long as product identification is based on *m/z* information only, since its product ion, the H_2Br^+, is also formed via the proton transfer between HBr^+ and neutral HBr present as background gas.[30] In the HBr^+ + DCl reaction system, the CT-channel is not directly accessible, since the DCl^+-signal overlaps with the H_2Cl^+-signal, which is formed via the proton transfer between HBr^+ and HCl. Hydrogen chloride is present due to the isotope exchange HBr + DCl ↔ DBr + HCl as well as the specified purity of the DCl-lecture bottle used (Sigma-Aldrich, 99 atom % D).

Ultimately, the HBr^+ + HCl (DCl) system offers the possibility to examine four reaction channels exhibiting considerably different thermochemical properties. While the PT-channels are strongly exothermic, the CT-channel is strongly endothermic. In contrast to that, deuterium abstraction (DA) is nearly thermoneutral.

Experiment and Simulation

Experimental approach

The cross sections presented in this study were measured inside a guided ion-beam (GIB) apparatus, which was described in earlier reports.[25,30] Hence, in the following, only aspects necessary for comprehension will be addressed. The apparatus consists of three zones: the ionization zone (IZ), the reaction zone (RZ) and the detection zone (DZ). In the IZ HBr^+-ions are formed by (2+1) resonance enhanced multiphoton ionization (REMPI). The reactant ions are accelerated towards the RZ by applying a specific repeller voltage, which defines the collision energy (E_{cm} = 0.25 eV to 5.85 eV for HBr^+ + HCl and E_{cm} = 0.12 eV to 2.03 eV for HBr^+ + DCl). The neutral reactant (HCl/DCl) is introduced into the RZ at room temperature by a dosing valve. Reactant ions and product ions are guided through the reaction zone by a linear octopole. The transfer of the ions into the DZ and thus into the quadrupole mass spectrometer (QMS) is realized by a transfer system consisting of an assembly of lenses and a conical octopole.[35] Ion signals are finally recorded by means of a multichannel scaler card (FAST ComTec, type: P7888). The kinetic data presented in this work are based on measuring all relevant ion signals, in particular the HBr^+, HCl^+, H_2Cl^+ signals including the natural isotopes of Br and Cl and the deuterium substitution. More details are given in the supplementary material.

The HBr-pressure in the IZ was typically set to $1.0 \cdot 10^{-5}$ mbar, whereas a HCl/DCl-pressure of $1.15 \cdot 10^{-4}$ mbar was applied to the RZ, ensuring single-collision conditions. The HBr^+-ions are formed rotationally state-selective via the F $^1\Delta_2$ ($v' = 0$) ← $^1\Sigma^+$ ($v'' = 0$) transition in the electronic and vibrational ground state ($^2\Pi_{1/2}$ ($v^+ = 0$)).[36] This leads to rotational state distributions dominated by two or three rotational states.[37] Using a tunable dye laser (Sirah Lasertechnik GmbH, type: Cobra-Stretch) operated with Coumarin 500 dissolved in Ethanol and pumped by a 20 Hz Nd:YAG-laser (Spectra-Physics Inc., type: Quanta Ray INDI), the (2+1)-REMPI-process is carried out. For the reactant ion, the $^2\Pi_{1/2}$-state was chosen instead of the $^2\Pi_{3/2}$-state, since the efficiency of the charge-transfer reaction for HBr^+ ($^2\Pi_{3/2}$) is too low in order to achieve an adequate statistical accuracy. A specific mean rotational energy of the ion is selected by addressing the appropriate pump-line in the REMPI-spectrum.

In case of the HBr^+ + HCl-system, the transitions R(1), R(3), R(4), R(5) and R(6) were used to vary the rotational energy between 3.4 meV and 46.8 meV. The R(2)-transition was not used for preparation of the ions since it overlaps with the S(0)-transition. For the HBr^+ + DCl-system, the rotational energy was varied

within the same range. Because of the overlap of the (2+1)-REMPI-spectra of DBr and HBr and isotope exchange of the reactants, the transitions Q(2), Q(3), Q(5), Q(6) and Q(7) were used. The mean rotational energies defined by R(J'') are similar to those defined by S(J'' - 1), where J'' represents the total angular momentum quantum number of the initial state concerning the REMPI-process.[37] Based on this finding, the mean rotational energies defined by R(J'') were assumed for Q(J'' + 1), since no rotational state distributions have been reported for the Q-branch. The R-branch was not used in case of HBr^+ + DCl because of the isotope exchange HBr + DCl ↔ DBr + HCl. The R(1)-transition for HBr^+ ($^2\Pi_{1/2}$) overlaps with the Q-branch of DBr^+ ($^2\Pi_{1/2}$), while the R(5)-transition of HBr^+ ($^2\Pi_{1/2}$) overlaps with the R(6)-transition of DBr^+ ($^2\Pi_{1/2}$). Since the intensity of R(7) is too low to achieve adequate statistical accuracy, the Q-branch was chosen for the cross section measurements. Concerning this branch, five transitions are suitable for *σ*-measurements regarding intensity and spectral purity. The Q(4)-transition was not considered since it overlaps with the P(5)-transition of DBr^+ ($^2\Pi_{1/2}$).

All *σ*-measurements regarding the same reaction system were performed with similar total ion signals, which were set in a way that Coulomb repulsion is negligible[38] and detector saturation is ruled out. The second-order rate constant k_i , where i indicates the channel, is given in eq (1) for the general case. The derivation beginning at the second order rate law is elaborated in the supplementary information.

$$k_{\mathrm{i}} = \frac{k'_{\mathrm{tot}} \cdot f . a_{.\mathrm{product}}}{1 - \exp(-k'_{\mathrm{tot}} \cdot t)} \cdot \frac{1}{[\mathrm{Neutral}]} \quad (1)$$

Rate constants k_{i} are transformed to cross sections via eq (2) implying the assumption that the neutral molecule is at rest and the kinetic energy of the ion equals the energy joined by acceleration.

$$\sigma = \frac{k}{v_{\mathrm{HBr^+}}} \quad (2)$$

Experimental cross sections are compared to Langevin-, ADO-(Average Dipole Orientation) and parameterized trajectory calculations based on the Su-Chesnavich model (labeled SC throughout the rest of the text). According to the Langevin-model, the cross section of an ion-molecule reaction is given by [39,40]

$$\sigma_L(E_{cm}) = \pi \cdot \left(\frac{2 \cdot \alpha \cdot q^2}{E_{cm}}\right)^{0.5} \quad (3)$$

Besides the charge *q* of the ion, the equation contains the polarizability *α* of the neutral molecule. The Langevin cross section σ_L scales with $E_{cm}^{-0.5}$ and is considered as an upper limit (Langevin-limit) in the case of a polarizable target since, according to the model, every collision leads to a reaction.

For target molecules with permanent dipole moment Su and Bowers developed the more sophisticated ADO-theory.[41] The ADO cross section σ_{ADO} additionally includes the dipole moment μ_D of the neutral molecule:

$$\sigma_{\mathrm{ADO}}(E_{\mathrm{cm}}) = \pi \cdot \left(\frac{2 \cdot q^2}{E_{\mathrm{cm}}}\right)^{0.5} \cdot \left(\alpha^{0.5} + C \cdot \mu_{\mathrm{D}} \cdot \left(\frac{2}{\pi \cdot k_B \cdot T}\right)^{0.5}\right) \quad (4)$$

Since the rate constant k_{ADO} is based on thermally averaged velocities, the Boltzmann constant k_B and the temperature *T* appear in the equation as well. A parameter *C* with values between 0 and 1 is introduced. It describes how strongly the dipole is oriented towards the ionic charge. If the angle *ϑ* between the vector of the dipole moment and the line connecting the centers of both reactants is 0°, the dipole is oriented fully towards the ionic charge and *C* equals 1. For the reaction system HBr^+ + HCl/DCl, *C* equals 0.1724.[42] Due to the inclusion of the attractive charge-dipole interaction, the ADO-model leads to larger cross sections compared to the Langevin-model.

Just as σ_L, σ_{ADO} scales with $E_{cm}^{-0.5}$. In addition, experimental cross section data are fitted to eq. (5):

$$\sigma \quad (E_{\mathrm{cm}}) = A \cdot \left(\frac{1}{E_{\mathrm{cm}}}\right)^n \quad (5)$$

This fit function consists of two fit parameters, namely *A* and *n*. The *A*-parameter reflects all system-specific constants. The parameter n reflects the de facto deviation from ideal Langevin / ADO behavior with *n* = 0.5.

The SC model is based on a Hamiltonian which consists of the following effective interaction potential V_{int} that also forms the basis for the ADO-theory:[43]

$$V_{\mathrm{int}} = -\frac{\alpha \cdot q^2}{2 \cdot r^4} - \frac{q \cdot \mu_{\mathrm{D}}}{r^2} \cdot \cos\theta + \frac{L^2}{2 \cdot \mu \cdot r^2} \quad (6)$$

The last summand represents the centrifugal potential containing the orbiting angular momentum L. The distance between the centers of both reactants is represented by r, whereas the reduced mass is described by μ. Trajectories, obtained by solving the Hamilton equations of motion have been parameterized by Su and Chesnavich with focus on the temperature dependence of the rate constant.[44] The SC cross sections presented in this study are based on that parameterization. An overview on capture theory models has been reported recently [45].

Ab initio molecular dynamics simulation

An accurate potential energy profile of the HBr^+ + HCl reaction has been previously characterized at the CCSD(T)/cc-pVDZ//CCSD(T)/CBS level by Fujioka et al..[46] In the current work, this reaction is studied with AIMD simulation, in which the system is propagated iteratively based on the force computed on the fly using quantum chemistry methods. After comparing various combinations of the DFT/MP2 and basis sets, frozen-core (FC)mp2[47]/aug-pc-1[48] and FCmp2/def2-SVP[49] were reported to be the optimal methods for AIMD.[46] As they had comparable levels of accuracy, FCmp2/def2-SVP was used here for its efficiency. For the AIMD trajectories, the two reactants'

initial conditions are chosen to replicate specific experimental conditions. For the HBr^+, J=0 and J=6 is used to mimic the experimental rotational energy of 0 and 0.05 eV, respectively. For the HCl (Θ_{rot} = 15.2 K),[50] which was introduced at room temperature (~298 K) in the experiment, the most probable state for HCl (J=3) is chosen. Both HBr^+ and HCl are set to their vibrational ground states. The collision energy between HBr^+ and HCl is specified as lowest collision energy in the experiment, 0.25 eV. As such, trajectories with a rotational energy of 0.00 eV (J=0) for the HBr^+ (i.e., a total of 0.25 eV excess energy) and 0.05 eV (J=6) for the HBr^+ (i.e., a total of 0.30 eV excess energy) comprise sets A and B, respectively. In addition, another set (C) of trajectories, with initial conditions of 0.30 eV collision energy and 0.00 eV rotational energy (J=0) for the HBr^+ (i.e., a total of 0.30 eV excess energy) is simulated. Set C aims to compare with Set B to investigate whether rotation impacts the reaction through additional excess energy or in a more specific manner. At the beginning of the AIMD simulations, HBr^+ and HCl are separated by a center of mass distance of 8 Å with the orientation between them sampled randomly.

A chemical dynamics software, VENUS[51], is employed to prepare the initial condition and the propagation of the trajectories, which is interfaced with a quantum chemistry software, NWChem[52], to calculate energy gradients necessary for the numerical integration[53]. A velocity Verlet integrator is used with a time step of 0.5 fs which can be lowered if the total energy of a trajectory is not stable. Trajectories are stopped when any two atom(s) are separated by a distance larger than 10 Å. The outcome of the trajectories is assigned with distance-based clustering as well as the partial charge of each atom estimated by Mulliken population analysis (i.e., to distinguish the reactants, HBr^+ + HCl, from the CT products, HBr + HCl^+). The impact parameter b is sampled at discrete values, starting with 1.0 Å. The number of trajectories N(b) at each b value increases linearly with b (i.e. N(b) ∝ b), starting with N(1.0 Å) = 40 with an increment of Δb = 1.0 Å [54]. The sampling stops at b_{max}, the largest impact parameter that a reactive trajectory is observed among 100 trajectories. Similar sampling procedures have been employed and produced trustworthy dynamics for ion-molecule reactions in the past[54,55,56,57]. For each set of initial conditions, the reaction probability vanishes at a maximum impact parameter b_{max} of 6.0 or 7.0Å (see Table 3) which results in a sampling of a total of 2280 trajectories. The intermediate and product/reactant assignment is done at each frame of the trajectory, which is determined by the minimal distance matrix deviation (DMD) among all DMDs between the structure found in the current frame of a trajectory (q) and the optimal structure of each intermediate and product/reactant. In this way, the pathway of each trajectory is described, and approximated lifetimes of each intermediate is calculated.

Results for HBr^+ + HCl

Experimental results

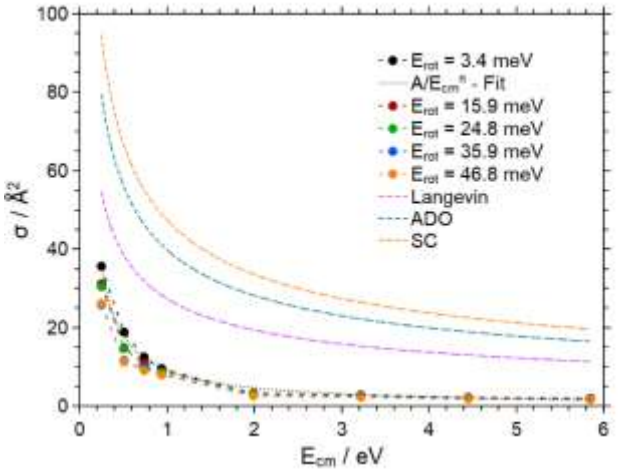

Figure 1. Cross sections for the PT_{HCl}-reaction as a function of the collision energy. The different traces correspond to different rotational energies. The dotted line represents the Langevin-fit. For error bars c.f. Figure 2.

In the HBr^+ + HCl reaction system the PT and the CT channel are experimentally observable and discussed below in this order.

In Figure 1, the cross section $\sigma_{PT,HCl}$ of the PT_{HCl}-reaction is plotted as a function of the collision energy E_{cm}. The different traces correspond to different rotational energies E_{rot} of the ion. As an example, the data for E_{rot} = 3.4 meV are provided with a fit according to eq. 5. Additionally, cross sections calculated according to the ADO- and the Langevin-model as well as the Su-Chesnavich model are displayed. The cross section $\sigma_{PT,HCl}$ decreases monotonically with increasing E_{cm}. This meets the expectations, since the PT_{HCl}-reaction is exothermic and barrierless. The decrease flattens out considerably for E_{cm}-values higher than 1.99 eV. All measured cross sections – which range from 1.55 Å² to 35.6 Å² – lie below the Langevin-limit. The ratio $\sigma_L/\sigma_{PT,HCl}$ varies between 1.5 and 6.3 depending on the collision energy. The ratios $\sigma_{ADO}/\sigma_{PT,HCl}$ and $\sigma_{SC}/\sigma_{PT,HCl}$ are even

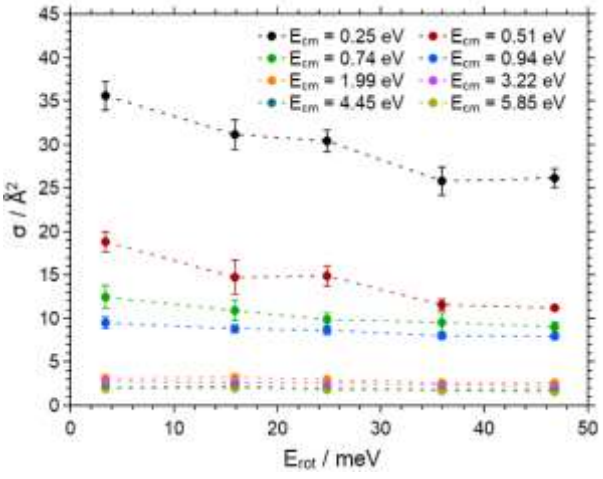

Figure 2. Cross sections for the PT_{HCl}-reaction as a function of the rotational energy. The different traces correspond to different collision energies.

larger, since the ADO-theory and the SC-model both include the dipole moment of the neutral reactant.

In Figure 2, the cross section $\sigma_{PT,HCl}$ is plotted as a function of the rotational energy for various collision energies.

The efficiency of the proton transfer reaction decreases with increasing rotational excitation of the ion. This trend is most obvious for the two lowest collision energies. The smallest E_{cm} shows a minor increase of σ between E_{rot} = 35.9 meV and E_{rot} = 46.8 meV. This increase is not significant within the error margins of the experiment.

In Table 1 the *n*- and *A*-parameters obtained by applying fits according to eq. 5 to the cross section data are shown. Generally, all *n*-values are larger than 0.5. Thus, the decrease of the experimental σ with increasing collision energy is steeper than predicted by the ADO- and the Langevin-model.

Table 1 Values for the exponents n in eq. 5 for different rotational energies.

E_{rot}/meV	$A_{PT,HCl}$	$n_{PT,HCl}$
3.4	9.1 ± 0.4	0.99 ± 0.03
15.9	7.9 ± 0.3	0.99 ± 0.03
24.8	7.6 ± 0.2	1.00 ± 0.03
35.9	6.7 ± 0.4	0.97 ± 0.05
46.8	6.4 ± 0.4	1.00 ± 0.05

Concerning the various rotational energies, the *A*-parameter scales with the largest observable cross section. Thus, *A* as a function of E_{rot} shows the same trend as σ vs. E_{rot}. Consequently, in consideration of the error margins, $A_{PT,HCl}$ decreases with increasing rotational energy.

The second reaction channel analyzed for the HBr^+ + HCl system is the CT channel. Overall, the cross sections are a factor of 100 – 10000 smaller than those for PT discussed above. The σ_{CT} data are shown in Figure 3 as a function of E_{cm}.

Since the CT-channel exhibits a positive reaction enthalpy (ΔH_{CT} = 0.76 eV), σ_{CT} increases with increasing translational energy. So σ_{CT} and $\sigma_{PT,HCl}$ show contrary trends in this context. In the E_{cm}-range from 0.25 eV to 0.74 eV, σ_{CT} increases only modestly with increasing E_{cm}. For E_{cm} > 0.74 eV, this increase becomes considerably steeper. The measured σ_{CT}-values range from 0.003 Å² to 0.093 Å². Comparing the respectively largest cross section for both channels, σ_{CT} and $\sigma_{PT,HCl}$ differ by three orders of magnitude. Figure 3 clearly shows, that the CT-reaction is also weakly observed for E_{cm}-values lower than the thermochemical threshold ($E_{cm} = \Delta H_{CT}$). In the following this will be rationalized by taking the respective E_{cm}-probability distributions into account.

All denoted, E_{cm}-values in this study (nominal collision energies) represent the collision energies where the corresponding E_{cm}-distributions peak. In Table 2 the E_{cm}-width at half-maximum ($FWHM_{Ecm}$) is shown together with the individual contributions of the ion and the neutral target for different nominal collision energies.

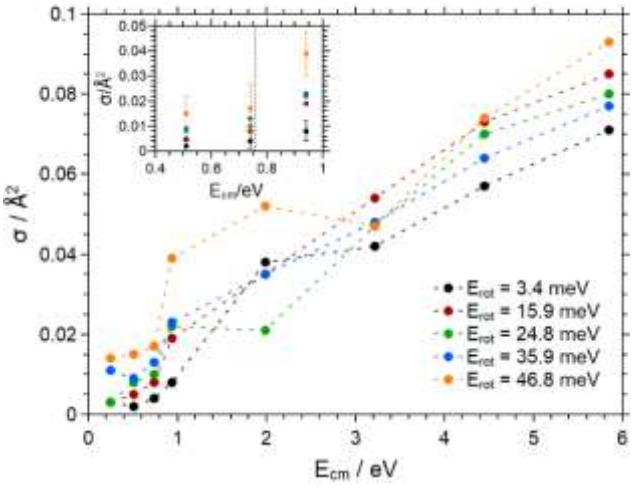

Figure 3. Cross sections for the CT reaction as a function of the collision energy. The different traces corresponds to different rotational energies. In the inset the cross sections are shown near the thermochemical barrier to show the rotational enhancement.

Table 2. E_{cm}-width for different collision energies for T = 293.15 K, supplemented by the individual contributions of the ion and the neutral target.

E_{cm}/eV	$FWHM_i$	$FWHM_n$	$FWHM_{Ecm}$/eV
0.25	0.059	0.22	0.23
0.51	0.15	0.31	0.35
0.74	0.22	0.38	0.44
0.94	0.31	0.43	0.52
1.99	0.59	0.62	0.86
3.22	0.97	0.79	1.25
4.45	1.34	0.93	1.63
5.85	1.77	1.06	2.06

The full width at half maximum of the kinetic energy distribution of the ion in the center of mass frame is represented by $FWHM_i$ (value obtained experimentally), whereas $FWHM_n$ – calculated according to equations (7) and (8) – originates from the thermal motion of the neutral target. The masses of the ion and the neutral species are represented by m_i and m_n respectively:[58]

$$\mathrm{FWHM_n} = (11.1 \cdot \gamma \cdot k_B \cdot T \cdot E_{cm})^{0.5} \quad (7)$$

$$\gamma = \frac{m_i}{m_i + m_n} \quad (8)$$

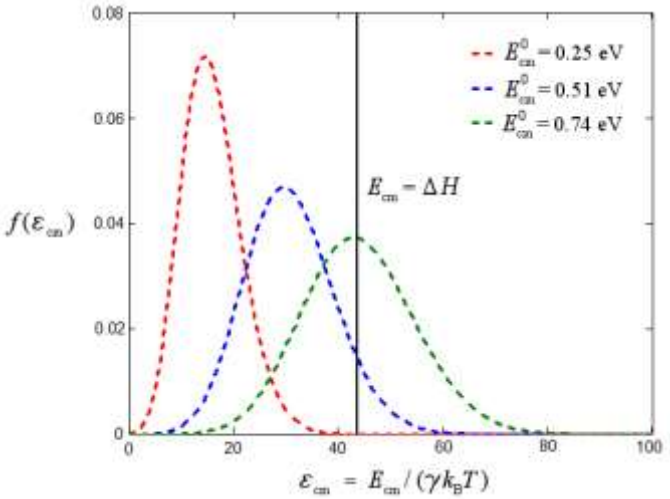

Figure 4. E_{cm}-probability distributions for the nominal collision energies of 0.25 eV, 0.51 eV and 0.74 eV.

The kinetic energy distribution of the ion is represented by a Gaussian function, whereas the thermal motion of the neutral target is based on Maxwell-Boltzmann statistics.[58] By convoluting the Gaussian function with the Maxwell-Boltzmann function, the (non-symmetric) E_{cm}-distribution with a certain $FWHM_{Ecm}$ is obtained.[58] For E_{cm} = 0.74 eV, the corresponding collision energy distribution at half-maximum ranges from 0.54 eV to 0.97 eV. Therefore, the distribution reaches out considerably beyond the thermochemical threshold. For E_{cm} = 0.51 eV, the E_{cm}-distribution ranges from 0.35 eV to 0.70 eV at the level of half-maximum. Of course, the E_{cm}-base width is broader than the FWHM, so that there are E_{cm}-values above the thermochemical threshold. This statement can be confirmed by means of Figure 4. Here, the E_{cm}-probability distributions $f(\varepsilon_{cm})$ for the nominal collision energies of 0.25 eV, 0.51 eV and 0.74 eV are depicted, in which the nominal collision energies are denoted by E_{cm}^0 for the sake of clarity. The dimensionless energy ε_{cm} is calculated in the following way for T = 293.15 K:[58]

$$\varepsilon_{cm} = \frac{E_{cm}}{\gamma \cdot k_B \cdot T} \qquad (9)$$

Furthermore, the vertical black line represents the thermochemical threshold (ΔH_{CT}) of 0.76 eV. Concerning the nominal collision energies of 0.51 eV and 0.74 eV, parts of the corresponding energy distributions lie above $E_{cm} = \Delta H_{CT}$, which explains the observation of the CT-reaction. In contrast to that, the observation of the CT-reaction for the nominal collision energy of 0.25 eV is surprising, since the corresponding energy distribution does not reach out beyond the thermochemical barrier. Here, the rotational energy of the HBr^+ helps to overcome the endothermicity of the reaction.

Regarding Figure 3, another important aspect has to be discussed: In the region where the collision energy is near the thermochemical threshold, namely for E_{cm} = 0.51 eV, 0.74 eV and 0.94 eV, σ_{CT} increases monotonically with increasing rotational excitation. This rotational enhancement is significant in the sense that the respective error margins for E_{rot} = 3.4 meV and E_{rot} = 46.8 meV do not overlap. This finding is illustrated in the inset of Figure 3, where the σ_{CT}-values for E_{cm} = 0.51 eV, 0.74 eV and 0.94 eV are plotted together with the relevant error bars.

The described rotational enhancement is also depicted in Figure 5, where the cross section of σ_{CT} is shown as a function of the rotational energy. Overall, the mean cross sections increases with increasing rotational energy in particular for the small collision energies investigated. For the larger collision energies the trend is less clear and the variation of the data is on the same order of magnitude as the error margins.

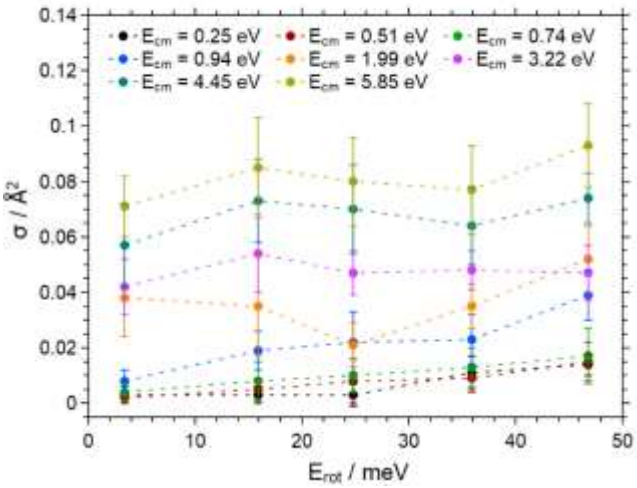

Figure 5. Cross sections for the CT-reaction as a function of the rotational energy. The different traces correspond to different collision energies.

Comparing the plots in Figure 2 (σ vs. E_{rot} – PT_{HCl}) and Figure 5 (σ vs. E_{rot} – CT) it becomes clear, that the error margins in case of PT_{HCl} are smaller than the ones for CT. The lower statistical accuracy in case of CT originates from the lower reaction efficiency and thus lower product ion yields.

AIMD Results

The reactive cross sections of various reaction pathways are shown in Table 3 alongside with the experimental results. Three different sets of calculations will be presented as outlined in the methodological section. For all three sets, all trajectories ended up either as HBr^+ and HCl or H_2Cl^+ and Br. While the latter results from a proton transfer (PT), the former could be either the result of a non-reactive (NR) collision or a hydrogen exchange (HE). Since the guided-beam experiment is not able to distinguish NR from HE, the cross section of HE is not reported. In regard to the charge transfer (CT) product, HBr and HCl^+, the guided beam experiment reports a cross section of up to four orders of magnitude smaller than PT, and it has not been observed in AIMD simulations. This is indeed a remarkable agreement since as shown in Table 3, there are roughly 650 reactive PT trajectories observed; thus, the expected number of CT trajectories observed is well below 1. Moreover, reactive CT

trajectories would not be expected here since the total available energy is below the threshold of the channel. In regard to the proton transfer (PT), by holding E_{trans} constant (0.25 eV) between sets A and B, the cross section decreases from 43.98 ± 2.13 Å^2 to 20.26 ± 1.53 Å^2, when E_{rot} increases from 0.00 eV to 0.05 eV. This observation qualitatively agrees with the decrease in experimental cross sections (35.59 ± 1.67 Å^2 to 26. 12 ± 1.06 Å^2) under the same condition. The moderate discrepancies are likely due to the difference in the excess energy in the system: although its average is the same, a relatively broad distribution in used in the experiment (see Fig. 3) but a fixed value is used in the AIMD simulations. For example, the lower rotational energy (0.00 eV, set A) was mimicked by setting J=0 for HBr^+ in all sampled trajectories, resulting in an expected E_{rot} of 0.0 eV. However, in the experiment, there was some population of higher J states due to the measured E_{rot} of 0.0034 eV. Thus, AIMD effectively uses an E_{rot} smaller than the guided-beam experiment, which results in an increased cross section. Further, for the E_{rot} =0.05 eV set of trajectories (set B), using the most probable rotational state for HBr^+ (J=6) and for HCl (J=3) does not perfectly replicate the experiment, which uses a mixture of J values for HBr^+ and a room temperature ensemble for HCl.

By holding E_{rot} constant (0.00 eV) between sets A and C, the cross section decreases from 43.98 ± 2.13 Å^2 to 38.33 ± 1.96 Å^2 when E_{trans} increases from 0.25 eV to 0.30 eV. The guided-beam experiment is not performed under the specific condition of set C, but an experimental cross section could be approximated from the best fit of various E_{trans} with E_{rot} = 0.00 eV. It turns out the decrease predicted by AIMD simulation (13%) is in excellent agreement with experiment (15.8%, from 35.59 ± 1.67 Å^2 to 29.97 Å^2). Overall, the AIMD simulation faithfully represents the dynamics observed in the guided-beam experiment under condition of low excess energy, specifically: 1) with the same E_{trans}, increasing E_{rot} decreases the cross section, 2) with the same E_{rot}, increasing E_{trans} decreases the cross section, and 3) the CT is a negligible for HBr^+ + HCl as compared to the PT pathway.

To further illustrate the different mechanisms operative, snapshots of representative PT pathways are shown in the top left panel of Figure 6. The PT pathway trajectories can be further broken down by their mechanism. A direct rebound (DR) mechanism, where Br immediately bounces back (opposite to the direction of incoming HBr^+) after the head-on collision, possesses an obtuse scattering angle (θ, its distribution is shown in the bottom right of Figure 6). As shown in the top right panel of Figure 6, DR is the dominating mechanism at low impact parameter. A direct stripping (DS) mechanism, where HBr^+ passes by HCl by its side and immediately offloads the proton to the Cl atom, possesses an acute scattering angle. DS is the dominating mechanism at large impact parameter.

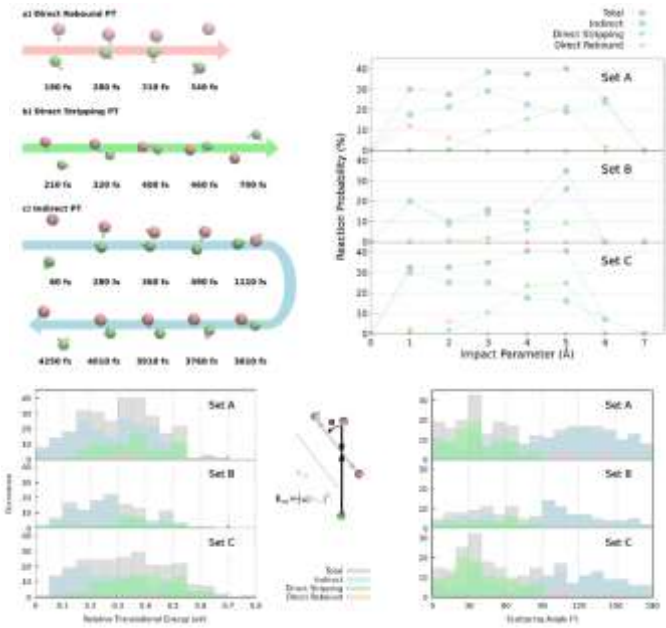

Figure 6. Representative AIMD trajectories are shown in the top left: a) a direct rebound proton transfer, b) a direct stripping proton transfer, and c) an indirect proton transfer. The reaction probability as a function of impact parameter is shown in the top right. After reacting, product molecules scatter and the angle between the final velocity of the Br and the initial velocity of the HBr^+ is depicted as θ (scattering angle) in the figure. The relative translational energy between the H_2Cl^+ and Br as well as the scattering angle are recorded and binned in histograms in the bottom left and right, respectively.

Table 3. Information about AIMD simulations. CE: the collision energy between HBr^+ and HCl; RE_{HBr+}: rotational energy of the HBr^+; N: the total number of trajectories sampled; b_{max}: the maximum impact parameter. The number of trajectories which underwent a proton transfer (PT), charge transfer (CT), or hydrogen exchange (HE) are listed as N^{PT}, N^{CT}, and N^{HE}, respectively. The computed cross sections σ_{comp} are listed alongside their closest experimental value σ_{exp}.

Initial Conditions					PT			CT			HE	
Set	CE / eV	RE_{HBr+} / eV	N	b_{max} / Å	N^{PT}	σ^{PT}_{comp} / Å^2	σ^{PT}_{exp} / Å^2	N^{CT}	σ^{CT}_{comp} / Å^2	σ^{CT}_{exp} / Å^2	N^{HE}	σ^{HE}_{comp} / Å^2
A	0.25	0.00	840	7.0	280	43.98 ± 2.13	35.59 ± 1.67	0	0.0	$3 \pm 3 \times 10^{-3}$	20	3.14 ± 0.70
B	0.25	0.05	600	6.0	129	20.26 ± 1.53	26.12 ± 1.06	0	0.0	$14 \pm 4 \times 10^{-3}$	11	1.73 ± 0.52
C	0.30	0.00	840	7.0	244	38.33 ± 1.96	n/a	0	0.0	n/a	15	2.36 ± 0.61

The DR and DS mechanisms are common in ion-molecule reactions[29,54,59–61]. The indirect (Ind) mechanism includes all those trajectories that experience a lifetime of the collision complex. Unlike DR or DS, trajectories with Ind mechanism are observed at all impact parameters and demonstrate a nearly isotropic scattering angle distribution. We note that in a limited number of cases (9% of the entire PT trajectories), the boundaries between direct (i.e., DR and DS) and Ind mechanism are somewhat blurry, as the lifetime of the collision complex could be very short. In such cases, conventions are employed to assist the assignment. For example, if the HBr^+ rotates around the HCl for at least three quarters of a circle, the trajectories are characterized as roundabout, falling into the Ind mechanism[62–64].

It is interesting to note that, in agreement with the experiments, the AIMD simulations show that the rotational excitation impacts this reaction more than just a source of excess energy – as an additional 0.05 eV in the form of rotational energy (comparing sets A and B) suppresses the reaction much more than the same amount of energy in the form of collision energy (comparing sets A and C). A detailed analysis shows the rotational excitation suppresses the direct mechanisms the most – comparing to set A, the probability of DS is at least halved for all impact parameters and DR is almost completely suppressed in set B. In comparison, the rotational excitation suppresses the Ind to a lesser degree. The rotational excitation also impacts the dynamics of the exit channel of the PT reaction. The kinetic energy of the products can be categorized into relative translational and internal (i.e., vibrational + rotational) energy, and the distribution of the relative translational energy is shown in the bottom left of Figure 6. Among all three mechanisms, the Ind on average preserves the least amount of relative translational energy (i.e., the collision is the least elastic). As demonstrated previously, the rotational excitation suppresses the direct pathways (DR and DS) more than it does to Ind pathways, thus the relative translational energy from set B, which has the largest portion of Ind, is the smallest among all three sets.

As seen in a previous AIMD study of HCl^+ + HCl, trajectories with less collision energy tend to more easily orient themselves away from a bimolecular collision leading to CT, and more towards PT. Consequently, the collision energy and CT cross section are negatively correlated. A similar trend can be seen with the rotational energy in the current study. The most straightforward comparison is between set A and B, where only the rotational energy of the HBr^+ differs; the largest contribution to the difference in reactive cross section is at b = 6.0 A (i.e., 25% reactive for set A and 0% reactive for set B). In those reactive trajectories, the HBr^+ and HCl preferentially orient themselves to form **i3** in ref. 46, which can then form the PT product, as illustrated in the bottom panel of Figure 7. The angle θ_{Br} describes the reactants' orientation and reactive trajectories (blue line, bottom panel) leading up to collision preferentially orient more towards **i3** (i.e., $cos(\theta_{Br}) \approx 1;\ \theta_{Br} \approx 0$). As the time derivative (top panel) illustrates, when averaged over the time leading up to collision, set A trajectories started with no rotational energy on the HBr^+, the landscape of the potential energy naturally brings them towards the **i3**-

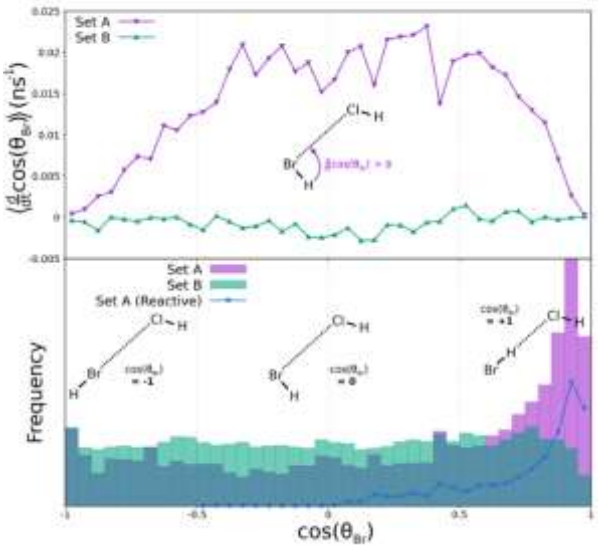

Figure 7. The angle θ_{Br} is calculated before collision. Top panel: the average time derivative of $cos(\theta_{Br})$ vs. θ_{Br}. Bottom panel, the probability distribution of $cos(\theta_{Br})$ vs. θ_{Br}. Data in this figure are taken over all trajectories at b=6.0 A for sets A and B (purple and green, respectively). The dotted line in the bottom panel indicates the same distribution but for the subset of reactive trajectories (blue).

orientation (i.e., the average time derivative of $cos(\theta_{Br}) > 0$). Set B trajectories, in the contrary, have enough rotational energy to fight again this preference and prevent the formation of **i3**, therefore there are no PT products observed.

Results for HBr^+ + DCl

This section presents results for the HBr^+ + DCl-system making reaction channels accessible which cannot be observed in the HBr^+ + HCl-system. In Figure 8, $\sigma_{PT,DCl}$ is shown as a function of E_{cm} for different rotational energies. Here, as an example an A/E_{cm}^n fit to the data for E_{rot} = 35.9 meV is also provided.

The cross section decreases monotonically with increasing collision energy, since the PT_{DCl}-channel is exothermic. In the E_{cm}-range from 0.12 eV to 2.03 eV, $\sigma_{PT,DCl}$ decreases from 32.6 Å^2 (at E_{rot} = 3.4 meV) to 1.96 Å^2. The lowest collision energy accessed for the PT_{HCl} channel was 0.25 eV giving rise to a cross section of $\sigma_{PT,HCl}$ = 35.6 Å^2. For the closest collision energy in the $\sigma_{PT,DCl}$ data, i.e. E_{cm} = 0.26 eV the cross section is $\sigma_{PT,DCl}$ = 22.1 Å^2.Thus, at small collision energy the proton transfer is significantly more efficient to HCl than to DCl. At large collision energies the two cross sections converge to a common value of approximately 2 Å^2.

Regarding the rotational dependence (see Figure 9), $\sigma_{PT,DCl}$ shows the same trend as $\sigma_{PT,HCl}$. The cross section decreases

with increasing ion rotation. This trend is the most obvious for the two lowest collision energies.

Figure 10 depicts the E_{cm}-dependence of the slightly exothermic

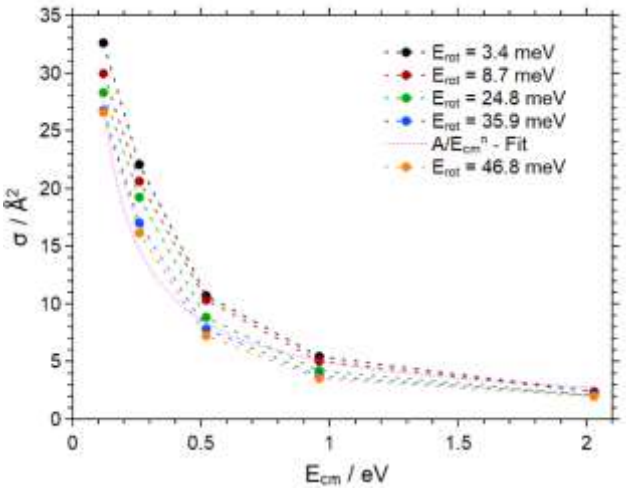

Figure 8. Cross sections for the PT_{DCl}-reaction as a function of the collision energy. The different traces correspond to different rotational energies. The dotted line represents the Langevin-fit.

DA-reaction. As an example, an A/E_{cm}^n fit to the data for E_{rot} = 8.7 meV is also provided. Clearly, the DA-channel shows an exothermic behavior, as σ_{DA} decreases with increasing collision energy. The measured cross sections are in the range of 0.08 Å² to 0.98 Å². Thus, the DA-reaction is less efficient than both PT-channels, but more efficient than the CT-channel. So overall, σ increases with decreasing ΔH.

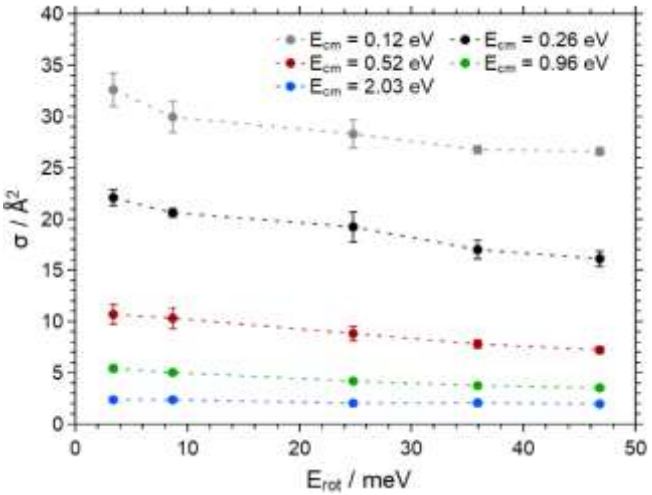

Figure 9. Cross sections for the PT_{DCl}-reaction as a function of the rotational energy. The different traces correspond to different collision energies.

In contrast to the other three reaction channels, the DA-reaction is independent of ion rotation within the scope of the error margins for all collision energies investigated (see Figure 11). The error margins are larger in comparison to the PT-channels due to lower product ion yields.

Comparing the rotational dependencies of σ_{PT} (see Figure 2 and Figure 9), σ_{DA} (see Figure 11) and σ_{CT} (see Figure 5), the following trend stands out: By going from an exothermic reaction (PT) via a quasi-thermoneutral reaction (DA) to an endothermic reaction (CT), the rotational trend changes from rotational hindrance via rotational independence to rotational enhancement. Thus, by going from $\Delta H < 0$ to $\Delta H > 0$, the rotational trend is inverted. Admittedly, the rotational enhancement regarding CT is mainly significant near the thermochemical threshold ($E_{cm} = \Delta H$). The results discussed above imply, that the dynamics is dominated by the overall reaction enthalpy and intermediate barriers as e.g. reported by Fujioka et al. [46] are not operative.

In Table 4 the *n*- and *A*-parameters obtained by applying fits

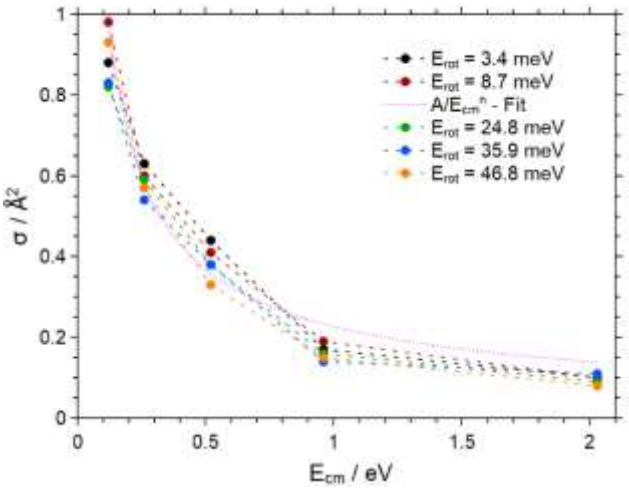

Figure 10. Cross sections for the DA-reaction as a function of the collision energy. The different traces correspond to different rotational energies. The dotted line represents the Langevin-fit.

according to eq. 5 to the cross section data are shown. Generally, all *n*-values are larger than 0.5. Thus, the decrease of the experimental σ with increasing collision energy is steeper than predicted by the ADO- and the Langevin-model

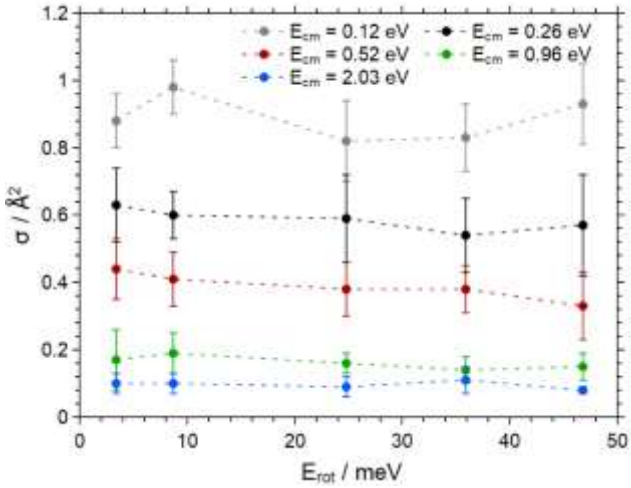

Figure 11. Cross sections for the DA-reaction as a function of the rotational energy. The different traces correspond to different collision energies.

respectively for both reaction channels. Concerning the various rotational energies, the *A*-parameter scales with the largest observable cross section. Thus, *A* as a function of E_{rot} shows the same trend as σ vs. E_{rot}. Consequently, in consideration of the error margins, $A_{PT,DCl}$ decrease with increasing rotational energy, whereas A_{DA} is independent of ion rotation.

Since *n* is larger than 0.5 for all three reaction channels, the decrease of the experimental cross section with increasing E_{cm} is always steeper compared to the ADO- and the Langevin-model. The major discrepancy is most evident for PT_{HCl}, since this reaction exhibits the largest *n*-values. By comparing Table 1 and Table 4 it is clear that the PT_{HCl}-channel exhibits the largest *n*-values ($0.97 \leq n_{PT,HCl} \leq 1.00$), whereas the lowest *n*-values belong to the DA-Channel ($0.62 \leq n_{DA} \leq 0.76$). Hence, the n_{DA}-values are closest to $n = 0.5$. Thus, the experimental data for the exothermic reaction in the undeuterated system shows a higher steepness compared to the reactions of the deuterated reactions, which show exothermic behavior.

Table 4. Values for the A-parameter in eq 5 for different rotational energies.

E_{rot}/meV	$A_{PT,DCl}$	A_{DA}	$n_{PT,DCl}$	n_{DA}
3.4	6.8 ± 1.2	0.24 ± 0.04	0.76 ± 0.10	0.62 ± 0.10
8.7	6.5 ± 1.2	0.23 ± 0.02	0.74 ± 0.10	0.70 ± 0.06
24.8	5.6 ± 1.2	0.22 ± 0.04	0.78 ± 0.11	0.64 ± 0.10
35.9	4.9 ± 0.8	0.21 ± 0.03	0.81 ± 0.09	0.66 ± 0.08
46.8	4.5 ± 0.7	0.19 ± 0.02	0.85 ± 0.08	0.76 ± 0.06

Discussion

In this section the results gained in this work will be compared to previous experimental and theoretical studies. In previous studies by the Weitzel group, self-reactions in the reaction systems HCl^+ (DCl^+) + HCl and HBr^+ (DBr^+) + HBr were investigated experimentally.[27,28,30] Concerning these systems, proton- and deuteron-transfer (PT and DT) on one side and hydrogen abstraction (HA) on the other side lead to the same product ion in each case (H_2Cl^+ (PT/HA), $HDCl^+$ (DT/HA), H_2Br^+ (PT/HA), $HDBr^+$ (DT/HA)). These product ions are formed exothermically.

Regarding the E_{cm}-dependence of the HCl^+ + HCl - system, the PT/HA- and the DT/HA-channel both show an approximate scaling of $\sigma \sim E_{cm}^{-2}$. The respective decrease of σ with increasing collision energy is less steep in case of the HBr^+ (DBr^+)-system with an approximate scaling of $\sigma \sim E_{cm}^{-0.5}$ to E_{cm}^{-1}. This is similar to the scaling of $\sigma_{PT,HCl}$, $\sigma_{PT,DCl}$ and σ_{DA} regarding the current study ($\sigma \sim E_{cm}^{-0.6}$ to E_{cm}^{-1}).

Regarding the E_{rot} dependence in HCl^+ + HCl, $\sigma_{PT/HA}$ runs through a minimum when plotted as a function of the rotational energy. This minimum occurs at E_{rot} = 32.5 meV and thus close to the rotational energy where the rotational velocities of the ion and the neutral molecule (ω_{ion} and $\omega_{neutral}$) are equal ($E_{rot} \approx 27$ meV). Looking at the deuterated reaction, equal rotational velocities exist for $E_{rot} \approx 52$ meV. Within the accessible E_{rot}-range from 0.5 to 42.5 meV, $\sigma_{DT/HA}$ decreases with increasing rotational excitation. The fact that no minimum occurs is in line with the position of equal rotational velocities lying beyond the accessible energy range.

As a next step the AIMD results obtained in this work for the HBr^+ + HCl reaction shall be compared to a previous theoretical study of a similar hydrogen halide bimolecular collision, HCl^+ + HCl[29]. In the latter system, the relative translational energy had been set to 0.2, 0.5, and 1.0 eV, while the rotational energy was kept at zero (*J* = 0). With respect to the PT reaction, both reactions share similar mechanism (DR, DS, and Ind) and demonstrate a similar level of negative correlation between the cross section and the relative translational energy (the slope of $\ln(\sigma)$ vs. $\ln(E_{cm})$ is 0.75 and 0.73 for HBr^+ + HCl and HCl^+ + HCl, respectively. See the Supporting Information for more details). With a similar level of excess energy, the cross section of PT of the HCl^+ + HCl collision (85.1 Å^2) [46] is overall larger than that of the HBr^+ + HCl reaction, which could be related to the energy difference in the exit channel: 0.55 eV for HCl^+ + HCl *vs.* 0.67 eV for HBr^+ + HCl. The impact of reaction energetics is demonstrated in the CT reaction in these two cases - the CT reaction of HCl^+ + HCl is isothermal and its cross section is non-negligible: 3.1 ± 0.8 (0.2 eV), 5.4 ± 1.1 (0.5 eV), and 3.7 ± 0.9 Å^2 (1.0 eV), which are 3.6%, 11.7%, and 14.2% of the cross section of the PT reaction under same condition. In the case of the HBr^+ + HCl, its CT reaction is highly endothermic (0.76 eV), and their cross section is four orders of magnitude smaller than the PT reaction according to the experiment and not detected in the AIMD.

Regarding the HBr^+ (DBr^+) + HBr -system, $\sigma_{PT/HA}$ as well as $\sigma_{DT/HA}$ exhibit a minimum when plotted against the rotational energy. However, in contrast to the HCl^+ (DCl^+) + HCl -system, the positions of the minima do not correlate with the ratio $\omega_{ion}/\omega_{neutral}$. In the current study, neither $\sigma_{PT,HCl}$ and $\sigma_{PT,DCl}$ nor

σ_{DA} exhibit a minimum within the accessible rotational energy range. In case of the HBr^+ + HCl-system, ω_{ion} and $\omega_{neutral}$ are equal for $E_{rot} \approx 33$ meV. Regarding the system HBr^+ + DCl, the respective E_{rot}-value is shifted to approximately 17 meV. In both cases, these rotational energy values lie in the accessible and investigated energy range. Already indicated in the HBr^+ (DBr^+) + HBr-study, the reaction system HBr^+ + HCl (DCl) now clearly emphasizes, that the relative rotational velocities are not the only contribution to the overall rotational dependence on the cross sections. To get a better understanding of the rotational effects observed, more AIMD simulations with systematic variation of the rotational excitation are required.[29,54]

Paetow et al. studied the reactions HBr^+ ($^2\Pi_i$) + $CO_2 \rightarrow HOCO^+$ + Br and DBr^+ ($^2\Pi_i$) + $CO_2 \rightarrow DOCO^+$ + Br, which are slightly endothermic for the HBr^+ spin-orbit ground state i=3/2, but exothermic for i=1/2.[25,26] There cross sections increased with increasing E_{cm} for the endothermic case and decreased with increasing E_{cm} for the exothermic case – as expected. In all cases the cross section decreased with increasing rotational excitation of the HBr^+ ion. In the current work the cross section also increased with increasing E_{cm} for the endothermic CT channel, but decreased with increasing E_{cm} for the exothermic PT and DA channel.

For the CT channel rotational enhancement is operative near the thermochemical threshold ($E_{cm} = \Delta H_{CT}$). Such a rotational enhancement near the thermochemical threshold was also found for the slightly endothermic reaction H_2^+ ($v^+ = 2$) + Ne $\rightarrow$ NeH^+ + H (ΔH = 0.014 eV) by Ng and co-workers.[24]

Summary

The cross sections for PT_{HCl}, PT_{DCl}, DA and CT in the HBr^+ + HCl (DCl)-system were measured inside a guided ion-beam apparatus under single-collision conditions. The HBr^+-ions were formed rotationally state-selective by resonance-enhanced multiphoton ionization (REMPI). In this way, the rotational energy E_{rot} was varied from 3.4 to 46.8 meV. In addition to E_{rot} the collision energy E_{cm} was varied from 0.25 to 5.85 eV in case of the undeuterated reaction system and from 0.12 eV to 2.03 eV in case of the deuterated one.

Regarding PT_{HCl} and PT_{DCl}, the cross section decreases with increasing collision energy. This is expected since both channels are exothermic. Although the DA-reaction is slightly endothermic, its efficiency decreases with increasing E_{cm}, mimicking an exothermic characteristic. In contrast to that, the slightly endothermic proton-/deuteron-transfer between HBr^+/DBr^+ ($^2\Pi_{3/2}$) and CO_2 showed characteristics of endothermicity.[25,26] The cross section for the CT-channel increases with increasing collision energy. This meets expectations, since the respective reaction enthalpy ΔH is markedly positive. The reaction channels PT_{HCl}, PT_{DCl} and DA all show a scaling of $\sigma \sim E_{cm}^{-0.6}$ to E_{cm}^{-1}, which is similar to the scaling of $\sigma_{PT/HA}$ and $\sigma_{DT/HA}$ regarding the HBr^+ (DBr^+) + HBr-system.[30] More specifically, the PT_{HCl}-channel shows the steepest decrease of the cross section with increasing E_{cm}. In contrast to that, the DA-efficiency shows the flattest decrease. As a consequence, the scaling of σ_{DA} matches the ADO- and the Langevin-model best. Comparing the absolute cross sections of PT, DA and CT, the reaction efficiency increases with decreasing ΔH. In contrast to the PT/HA-channel of HCl^+ + HCl[27] as well as the PT/HA- and the DT/HA-channel of HBr^+ (DBr^+) + HBr,[30] no minimum was found for either $\sigma_{PT,HCl}$ and $\sigma_{PT,DCl}$ or σ_{DA} as a function of E_{rot}.

Concerning the rotational energy dependence, PT_{HCl} and PT_{DCl} show a rotational hindrance in the experiment, whereas deuterium abstraction is independent of ion rotation. The endothermic CT-reaction shows a significant rotational enhancement near the thermochemical threshold ($E_{cm} = \Delta H$). Such a behavior was also found for the slightly endothermic proton transfer between H_2^+ ($v^+ = 2$) and Ne by Ng and co-workers.[24] Ultimately, by going from $\Delta H < 0$ (PT) via $\Delta H \approx 0$ (DA) to $\Delta H > 0$ (CT), the rotational trend observed in the experiment is inverted. The rotational enhancement of CT is mainly observed near the thermochemical threshold.

AIMD simulations were performed for the PT_{HCl} and CT reactions in the system HBr^+ + HCl. Both, the variation of the collision energy and of the rotational excitation of the HBr^+ ions have been taken into account. In particular for the PT_{HCl} reaction, a decrease of the cross section with both increasing collision energy and rotational excitation was found. The pivotal result is that the effect of rotational excitation is significantly larger than the effect of the same energy deposited in the cm collision. The CT reaction was observed experimentally 4 magnitudes smaller in efficiency than the PT_{HCl} reaction. This result is in accordance with the AIMD simulations, where 0 CT trajectory was observed in light of 650 reactive PT trajectories (e.g., leading to less than 1 reactive CT pathway expected). The AIMD trajectories have been used as the training set to construct a machine-learning potential energy surface which will be employed to conduct simulations of more E_{cm} and E_{rot} combinations as well as the DBr^+ + HCl system in the future.

Associated Content

There is Supporting Information electronically available as a separate file regarding the verification of single collision conditions and the analysis of the yields of reaction channels. Furthermore typical mass spectra of the reaction system are presented. Normalized experimental cross sections are shown and graphically compared to Langevin – theory for all channels investigated. Finally, AIMD cross sections for the title reaction, HBr^+ + HCl, are compared to previously reported data on the reaction HCl^+ + HCl.

Conflicts of interest

There are no conflicts to declare.

Author contributions

The experiments discussed have been conducted by D.P. and S.S., the AIMD calculations have been conducted by K.F.. The manuscript was written through contributions of all authors. All authors have given approval to the final version of the manuscript.

Funding Sources

Parts of this work have been supported by a grant from the Deutsche Forschungsgemeinschaft (We 1330-11). DP is supported by scholarship from the *Fonds der Chemischen Industrie* (FCI). Parts of this work has been supported by the National Science Foundation (USA) under Grant No. 2144031. The authors appreciate the information technology service (ITS) from the University of Hawai'i, Manoa for the computational resources.

References

1. M. Larsson, W.D. Geppert and G. Nyman, *Rep. Prog. Phys.*, 2012, **75**(6), 66901.
2. V.G. Anicich, P. Wilson and M.J. McEwan, *J. Am. Soc. Mass Spectrom.*, 2004, **15**(8), 1148.
3. W.K. Gichuhi and A.G. Suits, *J. Phys. Chem. A*, 2011, **115**(25), 7105.
4. Y. Xu, Y.C. Chang, Z. Lu and C.Y. Ng, *Astrophys. J.*, 2013, **769**(1), 72.
5. Y. Xu, B. Xiong, Y.C. Chang and C.-Y. Ng, *J. Phys. Chem. A*, 2018, **122**(32), 6491.
6. A.G. Suits, *J. Phys. Chem. A*, 2009, **113**(42), 11097.
7. E. Herbst, *Chem. Soc. Rev.*, 2001, **30**(3), 168.
8. D. Gerlich and S. Schlemmer, *Planet. Space Sci.*, 2002, **50**(12-13), 1287.
9. P. Allmendinger, J. Deiglmayr, O. Schullian, K. Höveler, J.A. Agner, H. Schmutz and F. Merkt, *ChemPhysChem*, 2016, **17**(22), 3596.
10. M.T. Bell, A.D. Gingell, J.M. Oldham, T.P. Softley and S. Willitsch, *Faraday Discuss.*, 2009, **142**, 73-91.
11. S. Schlemmer, E. Lescop, J. von Richthofen, D. Gerlich and M.A. Smith, *J. Chem. Phys.*, 2002, **117**(5), 2068.
12. D. Smith and N.G. Adams, *J. Chem. Soc., Faraday Trans. 2*, 1987, **83**, 149.
13. J. Perrin, O. Leroy and M.C. Bordage, *Contrib. Plasma Phys.*, 1996, **36**(1), 3.
14. E. Carrasco, M. Jiménez-Redondo, I. Tanarro and V.J. Herrero, *Phys. Chem. Chem. Phys.*, 2011, **13**(43), 19561.
15. M.S. Munson and F.H. Field, *J. Am. Chem. Soc.*, 1966, **88**(12), 2621-2630.
16. W. Lindinger, A. Hansel and A. Jordan, *Int. J. Mass Spectrom.*, 1998, **173**(3), 191.
17. P. Armentrout, *International Journal of Mass Spectrometry*, 2000, **200**(1-3), 219.
18. T. Glenewinkel-Meyer and D. Gerlich, *Isr. J. Chem.*, 1997, **37**(4), 343.
19. Y. Xu, B. Xiong, Y.-C. Chang, Y. Pan, P.K. Lo, K.C. Lau and C.Y. Ng, *Phys. Chem. Chem. Phys.*, 2017, **19**(15), 9778.
20. Y.C. Chang, Y. Xu, Z. Lu, H. Xu and C.-Y. Ng, *J. Chem. Phys.*, 2012, **137**(10), 104202.
21. Y. Xu, B. Xiong, Y.C. Chang and C.-Y. Ng, *J. Chem. Phys.*, 2012, **137**(24), 241101.
22. A. Li, Y. Li, H. Guo, K.-C. Lau, Y. Xu, B. Xiong, Y.-C. Chang and C.-Y. Ng, *J. Chem. Phys.*, 2014, **140**(1), 11102.
23. Y. Xu, B. Xiong, Y.C. Chang and C.-Y. Ng, *Phys. Chem. Chem. Phys.*, 2017, **19**(13), 8694.
24. B. Xiong, Y.-C. Chang and C.-Y. Ng, *Phys. Chem. Chem. Phys.*, 2017, **19**(28), 18619.
25. L. Paetow, F. Unger, W. Beichel, G. Frenking and K.-M. Weitzel, *J. Chem. Phys.*, 2010, **132**(17), 174305.
26. L. Paetow, F. Unger, B. Beutel and K.-M. Weitzel, *J. Chem. Phys.*, 2010, **133**(23), 234301.
27. T. Uhlemann, J. Wallauer and K.-M. Weitzel, *Phys. Chem. Chem. Phys.*, 2015, **17**(25), 16454.
28. T. Uhlemann, *Ionen-Molekül-Reaktionen in Gasphase von via REMPI zustandselektierten Ionen in den Reaktionssystemen H/DCl$^+$ + HCl und HCl$^+$ + H2 zur Untersuchung des Einflusses von Translations- und Rotationsenergie*. *Dissertation,* Marburg, 2015.
29. Y. Luo, T. Kreuscher, C. Kang, W.L. Hase, K.-M. Weitzel and R. Sun, *Int. J. Mass Spectrom.*, 2021, **462**(9), 116515.
30. S. Schmidt, D. Plamper, J. Jekkel and K.-M. Weitzel, *J. Phys. Chem. A*, 2020, **124**(41), 8461.
31. S.G. Lias, J.E. Bartmess, J.F. Liebman, J.L. Holmes, R.D. Levin and W.G. Mallard, *J. Phys. Chem. Ref. Data*, 1988, **17**, Supplement No. 1.
32. P. Botschwina, *J. Chem. Soc., Faraday Trans. 2*, 1988, **84**(9), 1263.
33. K.K. Irikura, *ApJ*, 2007, **36**(2), 389.
34. P. Botschwina, A. Zilch, P. Rosmus, H.-J. Werner and E.-A. Reinsch, *J. Chem. Phys.*, 1986, **84**(3), 1683.
35. M.A. Röttgen, K. Judai, J.M. Antonietti, U. Heiz, S. Rauschenbach and K. Kern, *Rev. Sci. Instrum.*, 2006, **77**(1), 13302.
36. M. Penno, A. Holzwarth and K.-M. Weitzel, *J. Phys. Chem. A*, 1998, **102**(11), 1927.
37. M. Penno and K.-M. Weitzel, *Z. Phys. Chem.*, 2004, **218**(3), 311.
38. S. Athenstädt, *Influence of the rotational quantum number on the ion-molecule reactions of state selected HBr$^+$-ions,* Marburg, 2007.

39. M.P. Langevin, *Ann. Chim. Phys.*, 1905, **5**, 245.
40. G. Gioumousis and D.P. Stevenson, *J. Chem. Phys.*, 1958, **29**(2), 294.
41. T. Su, *J. Chem. Phys.*, 1973, **58**(7), 3027.
42. T. Su and M.T. Bowers, *Int. J. Mass Spectrom.*, 1973, **12**(4), 347.
43. W.J. Chesnavich, T. Su and M.T. Bowers, *J. Chem. Phys.*, 1980, **72**(4), 2641.
44. T. Su and W.J. Chesnavich, *Journal of Chemical Physics*, 1982, **76**(10), 5183.
45. A. Tsikritea, J.A. Diprose, T.P. Softley and B.R. Heazlewood, *J Chem Phys*, 2022, **157**(6), 60901.
46. K. Fujioka, K.-M. Weitzel and R. Sun, *J Phys Chem A*, 2022, **126**(9), 1465.
47. M. Head-Gordon, J.A. Pople and M.J. Frisch, *Chemical Physics Letters*, 1988, **153**(6), 503.
48. F. Jensen, *Journal of Chemical Physics*, 2001, **115**(20), 9113.
49. F. Weigend and R. Ahlrichs, *Phys Chem Chem Phys*, 2005, **7**(18), 3297.
50. https://www.nist.gov/publications/nist-101-computational-chemistry-comparison-and-benchmark-database?pub_id=831580 (accessed August 8, 2022).
51. X. Hu, W.L. Hase and T. Pirraglia, *J. Comput. Chem.*, 1991, **12**(8), 1014.
52. M. Valiev, E.J. Bylaska, N. Govind, K. Kowalski, T.P. Straatsma, H. van Dam, D. Wang, J. Nieplocha, E. Apra, T.L. Windus and W.A. de Jong, *Computer Physics Communications*, 2010, **181**(9), 1477.
53. U. Lourderaj, R. Sun, S.C. Kohale, G.L. Barnes, W.A. de Jong, T.L. Windus and W.L. Hase, *Computer Physics Communications*, 2014, **185**(3), 1074.
54. Y. Luo, K. Fujioka, A. Shoji, W.L. Hase, K.-M. Weitzel and R. Sun, *J. Phys. Chem. A*, 2020, **124**(44), 9119.
55. J. Zhang, U. Lourderaj, R. Sun, J. Mikosch, R. Wester and W.L. Hase, *J Chem Phys*, 2013, **138**(11), 114309.
56. C. He, G.R. Galimova, Y. Luo, L. Zhao, A.K. Eckhardt, R. Sun, A.M. Mebel and R.I. Kaiser, *Proc Natl Acad Sci U S A*, 2020, **117**(48), 30142.
57. C. He, K. Fujioka, A.A. Nikolayev, L. Zhao, S. Doddipatla, V.N. Azyazov, A.M. Mebel, R. Sun and R.I. Kaiser, *Phys Chem Chem Phys*, 2021, **24**(1), 578.
58. P.J. Chantry, *J. Chem. Phys.*, 1971, **55**(6), 2746.
59. R.D. Levine, *Molecular Reaction Dynamics,* Cambridge University Press, 2005.
60. B.H. Mahan, *Acc. Chem. Res.*, 1968, **1**(7), 217.
61. R. Wolfgang, *Acc. Chem. Res.*, 1969, **2**(8), 248.
62. J. Mikosch, M. Weidemüller and R. Wester, *International Reviews in Physical Chemistry*, 2010, **29**(4), 589.
63. M. Paranjothy, R. Sun, Y. Zhuang and W.L. Hase, *WIREs Comput Mol Sci*, 2013, **3**(3), 296.
64. R. Sun, C.J. Davda, J. Zhang and W.L. Hase, *Phys Chem Chem Phys*, 2015, **17**(4), 2589.